RESEARCH ARTICLE

WILEY **NMR** IN BIOMEDICINE

Real-time multi-directional flow MRI using model-based reconstructions of undersampled radial FLASH – A feasibility study

Jost M. Kollmeier[1] (iD) | Zhengguo Tan[1] (iD) | Arun A. Joseph[1,2] | Oleksandr Kalentev[1] | Dirk Voit[1] | K. Dietmar Merboldt[1] | Jens Frahm[1,2]

[1] Biomedizinische NMR, Max-Planck-Institut für biophysikalische Chemie, Göttingen, Germany

[2] DZHK (German Centre for Cardiovascular Research), partner site Göttingen, Germany

Correspondence
J.M. Kollmeier, Biomedizinische NMR, Max-Planck-Institut für biophysikalische Chemie, 37070. Göttingen, Germany.
Email: jost.kollmeier@mpibpc.mpg.de

The purpose of this work was to develop an acquisition and reconstruction technique for two- and three-directional (2d and 3d) phase-contrast flow MRI in real time. A previous real-time MRI technique for one-directional (1d) through-plane flow was extended to 2d and 3d flow MRI by introducing in-plane flow sensitivity. The method employs highly undersampled radial FLASH sequences with sequential acquisitions of two or three flow-encoding datasets and one flow-compensated dataset. Echo times are minimized by merging the waveforms of flow-encoding and radial imaging gradients. For each velocity direction individually, model-based reconstructions by regularized nonlinear inversion jointly estimate an anatomical image, a set of coil sensitivities and a phase-contrast velocity map directly. The reconstructions take advantage of a dynamic phase reference obtained by interpolating consecutive flow-compensated acquisitions. Validations include pulsatile flow phantoms as well as in vivo studies of the human aorta at 3 T. The proposed method offers cross-sectional 2d and 3d flow MRI of the human aortic arch at 53 and 67 ms resolution, respectively, without ECG synchronization and during free breathing. The in-plane resolution was $1.5 \times 1.5 \text{ mm}^2$ and the slice thickness 6 mm. In conclusion, real-time multi-directional flow MRI offers new opportunities to study complex human blood flow without the risk of combining differential phase (i.e., velocity) information from multiple heartbeats as for ECG-gated data. The method would benefit from a further reduction of acquisition time and accelerated computing to allow for extended clinical trials.

KEYWORDS

model-based reconstruction, multi-directional flow MRI, phase-contrast MRI, real-time MRI

1 | INTRODUCTION

Dynamic phase-contrast (PC) flow MRI is a well-established technique for the quantitative assessment of cardiovascular blood flow. In comparison to Doppler ultrasound, PC flow MRI offers a free choice of the imaging plane without the need for an acoustic window and the option to quantify velocities in multiple directions. So far, however, adequate spatiotemporal resolution could only be achieved by ECG-synchronized acquisitions which unlike Doppler ultrasound average the MRI data over multiple heart cycles.[1] Extensions to multi-directional flow are desirable, e.g. for quantifying peak velocities in aortic valve stenosis,[2] but further increase the number of flow-encoding datasets which in turn prolongs the acquisition time and the effective temporal footprint for a velocity determination.

Progress has been made to accelerate PC MRI using non-Cartesian k-space trajectories[3,4] and advanced reconstruction techniques for parallel imaging.[5-7] Nevertheless, these accelerated cine MRI techniques still rely on a physiological gating strategy and therefore preclude, for example, a direct visualization of cardiovascular responses to stress or physical exercise and also hamper studies of patients with arrhythmias.

As an alternative, real-time PC MRI of blood flow, originally introduced by Riederer et al.,[8] aims at continuous imaging to resolve beat-to-beat variations of cardiac outflow without the need for ECG synchronization or breath holding. Using spiral acquisitions at 180 ms resolution Nayak et al.[9] achieved higher frames rates by a sliding-window reconstruction. Further advances were achieved with the use of a low-rank constraint on continuously acquired data sets,[10] although the retrospective nature of the approach does not allow for online reconstruction and display.

Recently, considerable progress in real-time MRI based on regularized nonlinear inverse reconstructions (NLINV) of highly undersampled radial gradient-echo acquisitions drastically increased the temporal resolution of cross-sectional image series.[11,12] The basic approach could be extended to real-time PC flow MRI at 35 to 40 ms resolution[13,14] for one-directional velocity encoding (i.e., through-plane flow), while the subsequent development of a model-based reconstruction method achieved about 25 ms.[15] At the same time the model-based approach improves the spatial acuity because it results in velocity maps free of the usual phase noise in regions without signal support (e.g., the lungs).

This work attempts to exploit these advances for the development of a multi-directional PC flow MRI technique in real time. Future clinical applications might allow for a dynamic and flexible evaluation of fluid dynamics. The first steps presented here refer to the implementation of in-plane flow-encoding schemes in highly undersampled radial spoiled gradient-echo sequences also known as fast low angle shot (FLASH) sequences and the evaluation of a suitable model-based reconstruction. Experiments using pulsatile flow phantoms demonstrate the feasibility and accuracy of the proposed method, while preliminary studies of the human aorta explore its potential for a rapid evaluation of complex flow phenomena.

2 | THEORY

In PC flow MRI the echo time TE is usually chosen as short as possible in order (i) to secure short repetition times and achieve high temporal resolution, (ii) to support the assumption of a constant velocity during echo formation, and (iii) to prevent dephasing effects. The current implementations follow ideas originally developed by Bernstein et al.[16] who presented a method for designing flow-encoding gradients with minimized TE by merging flow-encoding and imaging gradients. While originally introduced for Cartesian sampling with a constant read gradient G_R, the latter rotates for radial sampling as a function of the projection angle φ. This rotation has to be taken into account when applying the method of[16] to radial imaging. Given the optimized gradient waveforms for a Cartesian readout with in-plane flow sensitivity in x-direction, the gradient amplitudes for radial sampling are modulated by:

$$G_R^X(\varphi) = G_R \cos(\varphi)$$

$$G_I^X(\varphi) = G_I \cos(\varphi) - 2M_V \frac{1 - \cos(\varphi)}{(w_o + w_I)(w_I - r)}$$

$$G_O^X(\varphi) = G_O \cos(\varphi) + 2M_V \frac{1 - \cos(\varphi)}{(w_o + w_I)(w_o - r)}$$

Here, r denotes the minimal gradient ramp-up and ramp-down time and w the duration of inner (i) and outer (o) gradient lobe. A brief derivation is given in the Appendix. For flow sensitivity in y-direction the corresponding gradient strengths may be obtained by replacing $\cos(\varphi)$ by $\sin(\varphi)$. The method enables the readout gradient strength to be modulated by the projection angle as necessary for radial sampling, while the first-order gradient moment responsible for flow encoding remains constant in x- or y-direction.

3 | METHODS

3.1 | Subjects

All measurements were performed on a MRI system operating at 3 T (Magnetom Prisma fit, Siemens Healthcare, Erlangen, Germany). For in vivo studies, 13 subjects without known heart disease were recruited. Written informed consent, according to the recommendations of the local ethics committee, was obtained from all subjects prior to MRI.

3.2 | Image acquisition

Real-time multi-directional PC flow MRI was based on highly undersampled radial FLASH sequences with uniform coverage of k-space and rotated sets of spokes in successive frames[12] as well as randomized RF spoiling.[17] A schematic RF pulse and gradient sequence is shown in Figure 1. Using in-plane flow sensitivity as described above, multi-directional flow-encoding was implemented as a simple four-point method[18] with a sequential acquisition scheme. The same 5 spokes were used for all flow-encoding steps with a 30% asymmetric echo.[14] The acquisition parameters for phantom and in vivo studies are summarized in Table 1. In order to avoid peripheral nerve stimulation and improve patient compliance in future clinical trials, in vivo studies deliberately employed a conservative gradient mode with reduced maximum slew rates. For example, real-time 2d flow MRI may be performed at 43 ms resolution, i.e. 23 frames per second (fps), when using the full gradient capabilities.

The proposed method was validated with the use of a computer-controlled pulsatile flow phantom consisting of a water hose (16 mm inner diameter) wrapped around a water-filled cylinder. Velocities along the tube were compared to a previously developed real-time through-plane flow MRI technique.[13-15] The multi-directional flow method was also applied to a more complex phantom based on a cylindrical water tank with tangential inlet. In vivo studies of real-time 2d flow, as an important step in the technical development, and 3d flow MRI focused on the aortic arch and covered several heart beats for at least 10 s periods during free breathing.

Phantom studies were conducted with a standard 64-channel head coil, while in vivo measurements were performed with an 18-element thorax coil in conjunction with suitable elements of the 32-element spine coil.
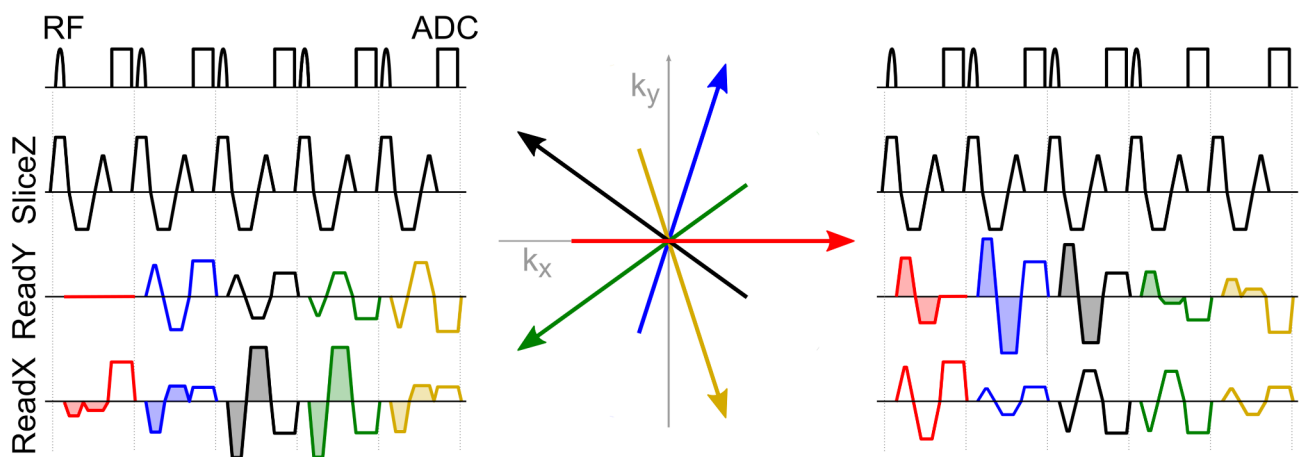

FIGURE 1 Schematic RF pulse and gradient sequence for real-time multi-directional PC flow MRI based on highly undersampled radial FLASH. (left) in-plane flow sensitivity in x-direction, (middle) radial sampling pattern for 5 spokes in k-space, and (right) in-plane flow sensitivity in y-direction. The shaded gradient lobes include the flow encoding. Individual colors indicate corresponding radial spokes

TABLE 1 Parameters for real-time multi-directional flow MRI

	Phantom		Aorta	
	1d flow	2d flow	2d flow	3d flow
Field-of-view/mm^2	192 × 192		320 × 320	
Image matrix	192 × 192		212 × 212	
Resolution/mm^2	1.0 × 1.0		1.5 × 1.5	
Slice thickness/mm	5		6	
Echo time/ms	2.55	2.54	2.46	2.50
Repetition time/ms	3.57	3.51	3.51	3.33
Bandwidth/Hz pixel^{-1}	840	930	815	1240
Flip angle/degree	10		12	
VENC/cm s^{-1}	100		200	
Spokes per flow-encoding dataset	5		5	
Acquisition time per frame/ms	36	53	53	67
Frames per second	28	19	19	15

3.3 | Image reconstruction

The model-based reconstruction applied here follows a recent development for through-plane flow MRI.[15] It jointly estimates a complex anatomical image, a phase-difference (i.e., velocity) map and a set of coil sensitivity maps. The corresponding nonlinear inverse problem is constrained by temporal regularization to the preceding frame and solved by the Iteratively Regularized Gauss-Newton Method. The method applies Tikhonov L2 regularization on all parameter maps and enforces the coil sensitivity maps to be smooth. The algorithm downsizes all regularization terms by a factor of two in each iterative step in order to ensure predominance of the data consistency term and to optimize temporal fidelity of the quantitative velocity data. Further details are given in.[12,15] To secure rapid convergence of the numerical optimization, the unknown velocity maps were scaled according to an automatic scaling technique.[19]

The aforementioned signal model applies to 1d flow comprising two differentially flow-encoded acquisitions. In contrast, multi-directional flow MRI relies on the acquisition of three or four encoding steps. In this work, all flow-encoded datasets share one reference scan (e.g., a flow-compensated acquisition) and the model-based reconstructions followed the 1d approach separately for each velocity component albeit with suitable reference data (see below). A common magnitude image for each time point was created by averaging the resulting two or three anatomical images.

An assumption of the PC signal model is that both encoding steps share the same image content and only differ with respect to the velocity-encoded phase information. For sequential acquisition schemes this assumption is well fulfilled when using only two encoding steps such as for 1d flow. For longer acquisitions using multi-directional flow encodings, and in particular for two encoding steps which do not directly follow each other in a 3d flow experiment, the image content is more likely to change during the prolonged time interval. To compensate for this effect and avoid violations of the signal model for reconstruction, the present work implemented a pre-processing step that adapts the phase reference for each flow direction individually. The procedure is outlined in Figure 2. The phase reference is interpolated by a linear combination of the two flow-compensated datasets from consecutive frames. The corresponding linear coefficients reflect the individual time gaps and are given by
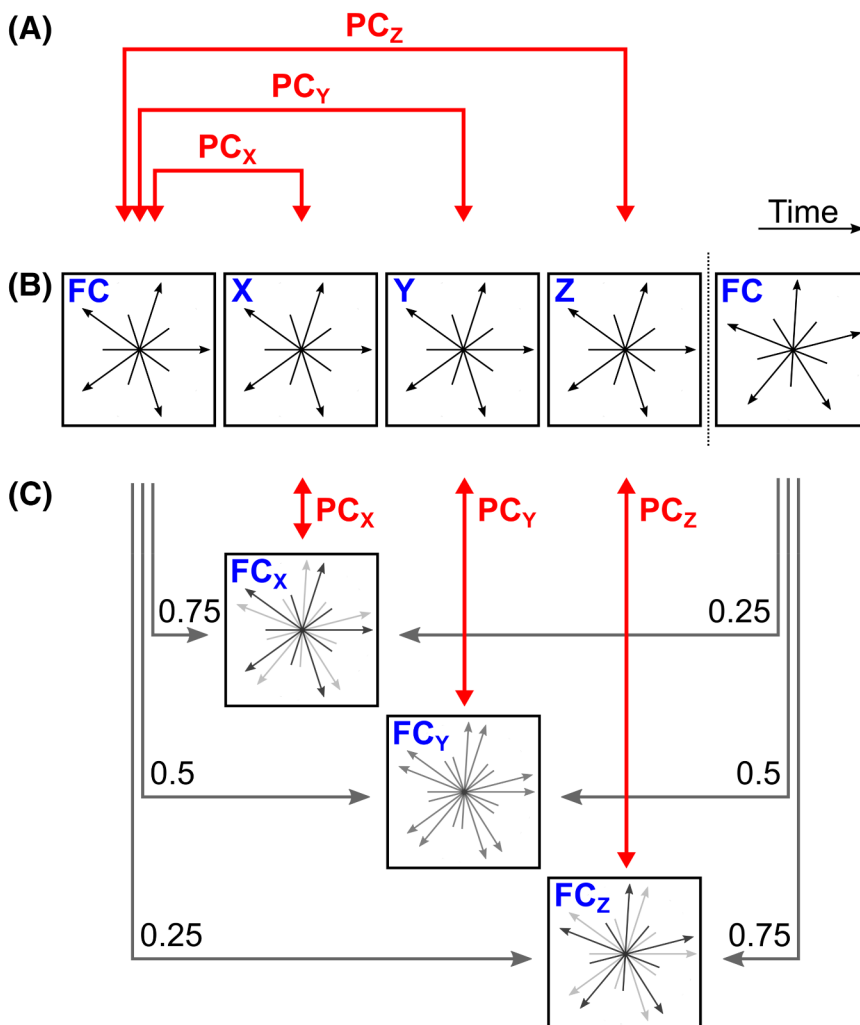

FIGURE 2 Phase references for 3d PC flow MRI in x, y, and z direction. (a) Conventional method, (b) serial flow-encoded and flow-compensated datasets, and (c) adaptive phase reference as obtained by interpolation of two consecutive flow-compensated (FC) acquisitions

$\left(1 - \dfrac{i-1}{N_E}\right)$ and $\dfrac{i-1}{N_E}$ where i denotes the index of the encoding step and N_E the total number of encodings. The model-based reconstructions for each flow direction then use the respective composite phase reference together with the original flow-encoded data.

At this stage all data processing was accomplished offline with a total reconstruction time of about 6 min for a 10 s MRI video. While gradient delay correction,[20] compression of the multi-coil raw data to 10 virtual coils by means of a principal component analysis, and convolution-based gridding without density compensation were done in MATLAB (MathWorks, Natik, MA), the main iterative optimization was implemented in C/CUDA (GeForce GTX TITAN, NVIDIA, Santa Clara, CA).

3.4 | Visualization of 2d flow

As a complementary tool for displaying 2d flow data within a single combined image, the implementation calculated a speed image which represents the root sum of squares of two perpendicular velocity components. It visualizes absolute velocities as brightness (magnitude of velocity vector) and includes the flow directions (vector orientation) by color coding. In addition, an overlay of the speed image with the corresponding T1-weighted magnitude image may add further insights resembling Doppler ultrasound. Because the almost noiseless PC maps require no masking, this overlay image I may easily be calculated by a linear combination of the speed image S and magnitude image M

$$I = s*S + (1-s)*M$$

where the linear coefficient s for each pixel is given by normalization of the speed image. This approach combines the information of both velocity maps and the anatomical image into a single image providing maximum flow information to the viewer.

4 | RESULTS

4.1 | Phantom studies

Figure 3 shows results obtained for real-time 2d flow MRI of a pulsatile flow phantom (see also Suppl. Video S1). Quantitative velocities along the tube (mean values within a selected region-of-interest) are compared to those obtained by real-time 1d flow MRI (parameters see Table 1). The close overlap of velocity time courses for 1d flow MRI after Gridding+FFT as well as for 1d and 2d flow MRI after model-based reconstruction demonstrates excellent agreement. Close reference to a Gridding+FFT solution confirms a proper choice of regularization strength and convergence of the iterative optimization problem which implicitly supports temporal fidelity.

As previously observed for real-time 1d flow MRI,[14] also model-based reconstructions for multi-directional flow MRI yield velocity maps of good image quality regarding the substantial degree of undersampling. In particular, the velocity maps offer high spatiotemporal resolution and are characterized by a lack of phase noise in regions without MRI signal support. This finding also holds true for a pulsatile flow phantom which leads to patterns of turbulent flow by tangential water injection into a cylindrical tank as depicted in Figure 4 (see also Suppl. Video S2). In addition to quantitative velocity maps, qualitative information about slow flow phenomena is obtained by the flow-sensitive nature of the serial magnitude images. Both aspects are captured by an overlay image (Figure 4e) which combines qualitative signal patterns reflecting flow-induced dephasing and T1 inflow effects with quantitative information about high velocities close to the chosen VENC. These overlay maps may be useful in practice as they compensate for the low velocity-to-noise ratio which is unavoidable for velocities much smaller than the VENC in PC flow MRI.

4.2 | Human studies

Real-time multi-directional flow MRI with and without adapted phase reference and individual model-based reconstructions was applied to the human aortic arch during free breathing in order to evaluate the performance of the adaptive phase reference and to validate the results in humans. Figure 5 shows selected through-plane velocity maps which are derived from 3d flow MRI studies with and without adaptation of the flow-compensated reference data. Because of the high velocities in the ascending aorta, magnitude images show significant variation due to the rapid inflow of unsaturated spins. As a consequence, the underlying dynamics are better represented by adapting the phase reference as proposed. In the velocity maps without reference adaptation the appearance of artifacts must be ascribed to violations of the signal model, while these problems are avoided using the proposed method. Little to no influence was observed on the quantitative data after ROI evaluation. Almost no differences were observed for the in-plane flow components (not shown), most likely because the corresponding time difference between the respective flow-encoding and flow-compensating datasets is smaller.

Figures 6 and 7 refer to peak-systolic frames selected from real-time 2d and 3d flow MRI of the aortic arch at a temporal resolution of 19 and 15 fps, respectively (see also Suppl. Videos 3 and 4). The figures summarize quantitative velocity maps with minimal artifacts and absence of phase noise. The speed image with color-coded flow directions in Figure 6d and, in particular, the overlay image in Figure 6e allows for a combined
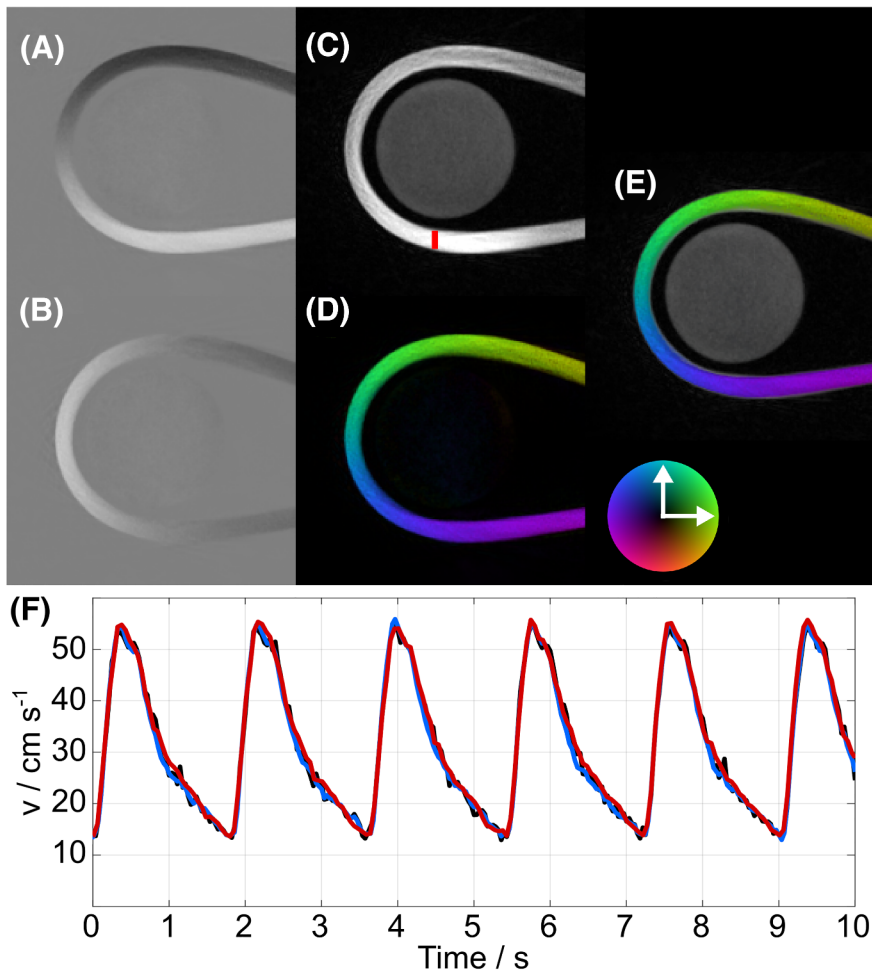
FIGURE 3 Pulsatile flow phantom. (a) Selected PC map in right–left direction, (b) PC map in up-down direction and (c) corresponding magnitude image obtained by real-time 2d flow MRI. (d) In-plane speed image with color-coded flow direction and (e) overlay image of (c,d). (f) Velocity time courses (ROI in c) obtained by 1d flow MRI after gridding+FFT (black) as well as by model-based 1d (blue) and 2d flow MRI (red)
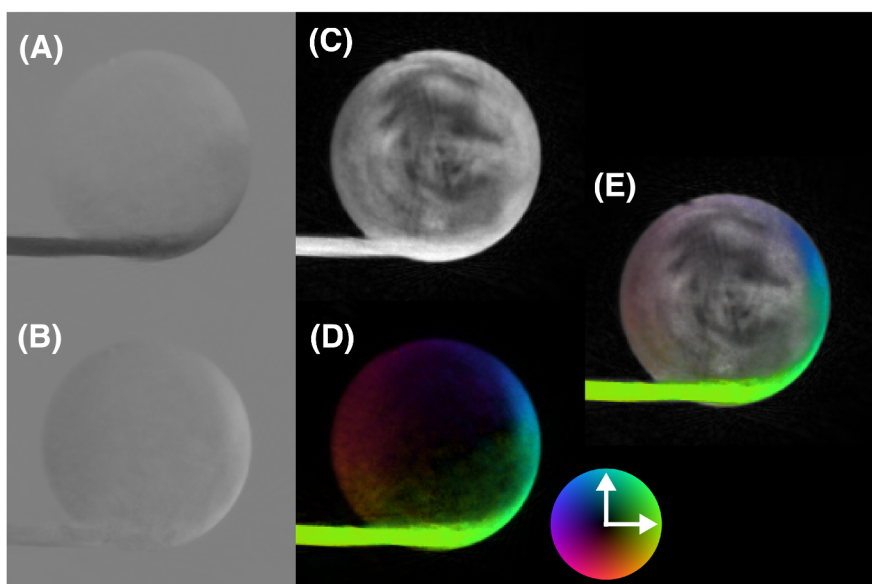

FIGURE 4 Pulsatile flow phantom with tangential flow injection. (a) Selected PC map in right–left direction, (b) PC map in up-down direction, and (c) corresponding magnitude image obtained by real-time 2d flow MRI. (d) In-plane speed image and (e) overlay image of (c,d)

representation of high in-plane velocities and slower turbulent components. Through-plane flow in the supra-aortic branches visible in the magnitude image is not well seen in in-plane flow maps. Figure 8 compares velocity time courses for real-time 2d and 3d flow MRI of the ascending and descending aorta. Though of limited temporal resolution, the resulting profiles reveal a distinct time difference between peak flow in the ascending and descending aorta and also indicate beat-to-beat variations during free breathing.
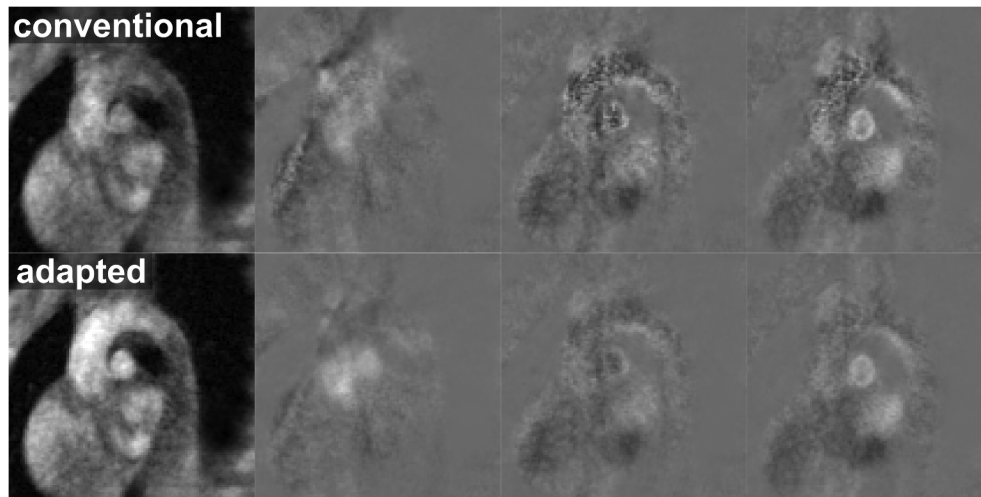
FIGURE 5   Effect of adaptive phase reference. Selected magnitude images and PC maps (through-plane flow component) of a real-time 3d flow MRI study of the aortic arch with (top) conventional method and (bottom) adapted phase reference. Differences due to inflow (magnitude image) and reconstruction artifacts (PC maps) are apparent which are avoided by a composite phase reference
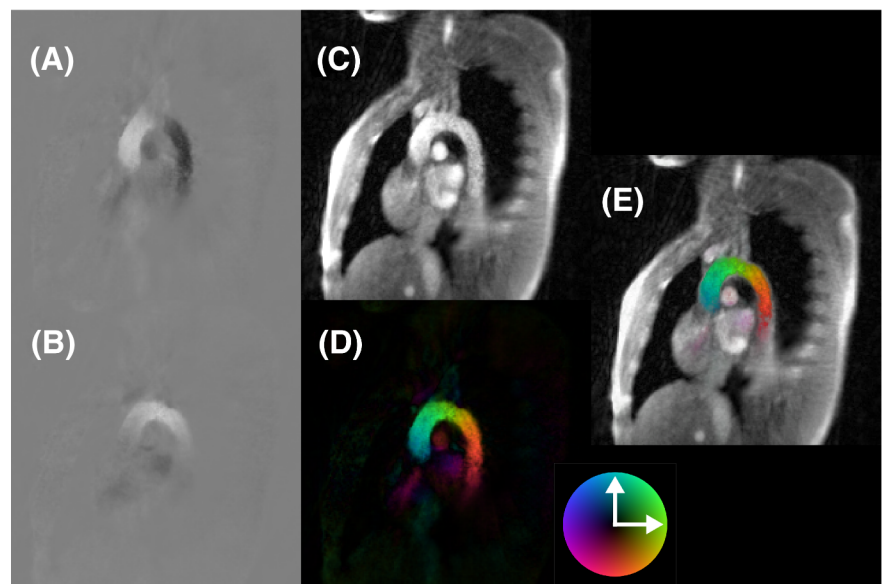

FIGURE 6   Peak-systolic frames of a real-time 2d flow MRI study of the aortic arch at 53 ms temporal resolution, i.e. 19 fps. (a) PC map in foot-head direction, (b) PC map in anterior–posterior direction, (c) magnitude image, (d) in-plane speed image, and (e) overlay image of (c,d)

Quantitative evaluations of peak flow velocities as determined by real-time 2d and 3d flow MRI for all 13 subjects are summarized in Table 2. The mean values were obtained for a continuous 10 s measurement in three positions along the ascending aorta and aortic arch (see Suppl. Figure S1). Apart from representing reasonable blood flow velocities for a group of young healthy volunteers, the data reveal a high degree of intra-subject consistency with no systematic quantitative differences between 2d and 3d flow MRI (see Suppl. Figure S2). However, in two subjects not all portions of the aorta could be sufficiently well (i.e., centrally) covered by the imaging plane, for example in the descending aorta (subject #2) and top position of the aortic arch (subject #4). In these cases no meaningful peak velocities from the central vessel lumen were available.

5 | DISCUSSION

This work demonstrates the first development of a real-time MRI method for the acquisition, reconstruction and display of multi-directional flow. Highly undersampled radial trajectories with only 5 spokes per encoding step achieve a temporal resolution of 53 and 67 ms (i.e., 19 and 15 fps) for cross-sectional 2d and 3d flow MRI, respectively. This is accomplished despite the use of conservative below-maximum gradients to avoid peripheral nerve stimulation under all circumstances. The approach benefits from minimized echo times which were obtained by overlapping flow-encoding and radial imaging gradients. Moreover, the implementation of a composite reference for the flow-compensated dataset reduces temporal inconsistencies which may occur due to rapid intensity changes. The procedure avoids corresponding violations of the used signal model
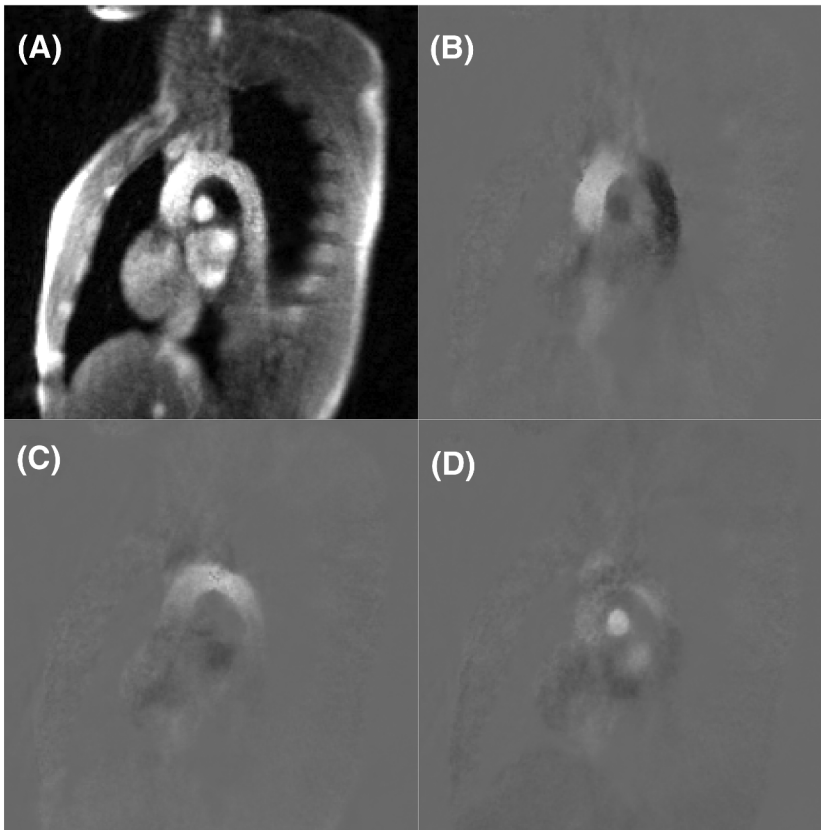
FIGURE 7 Peak-systolic frames of a real-time 3d flow MRI study of the aortic arch at 67 ms temporal resolution, i.e. 15 fps. (a) Magnitude image, (b) to (d) PC maps in foot-head, anterior–posterior and left–right (through-plane) direction, respectively
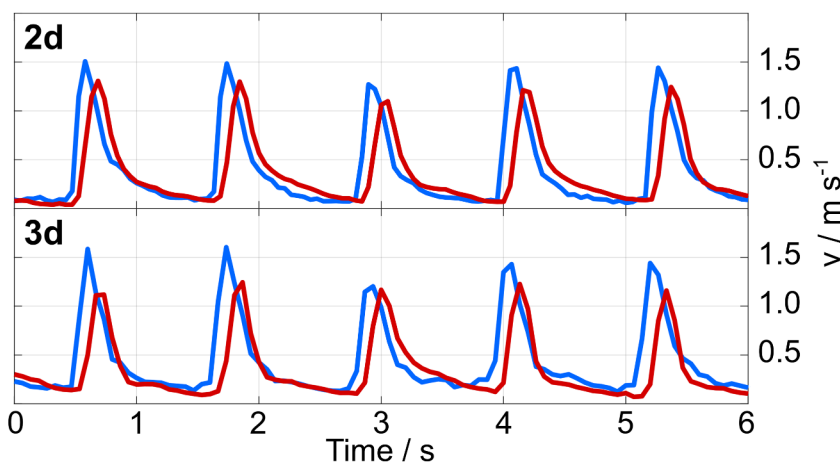

FIGURE 8 Velocity time courses in the ascending (blue) and descending aorta (red) for real-time 2d and 3d flow MRI at 53 ms and 67 ms resolution, respectively

for reconstruction which assumes the flow-encoded and flow-compensated datasets to share the same anatomical image. Phantom and in vivo studies resulted in good image quality as characterized by high spatiotemporal resolution and almost noiseless velocity maps in all directions.

While eddy-current induced gradient delays were properly dealt with using a pre-processing routine prior to gridding,[20] concomitant field contributions were neglected in the present study because of measurements in the high VENC regime (i.e., weak flow-encoding gradients) and the use of a conservative below-maximum gradient mode. In addition, concomitant field contributions tend to decrease for higher magnetic field strengths such as 3 T. Nevertheless, if necessary, a Maxwell correction can directly be included into the reconstruction process. Further developments may also adopt the use of complementary k-space data for different flow encodings similar to[21] or design a model-based reconstruction that jointly estimates two or all three components of the velocity vector. Another potential model extension allows for changes in the magnitude images representing flow-compensating and flow-encoding steps in order to account for dephasing effects caused by higher-order flow moments.

Multi-directional flow studies are commonly performed using ECG-gated 4D flow MRI.[22,23] Such studies typically cover a larger 3D volume which, for example, encompasses the entire aortic arch at isotropic spatial resolution. Although the proposed real-time flow MRI technique offers similar spatial resolution in terms of voxel sizes, both approaches exhibit fundamental differences. In particular, cross-sectional real-time 3d flow

TABLE 2 Peak velocities in the human aorta as obtained by real-time 2d and 3d flow MRI

Subject	2d flow			3d flow		
	Pos 1	Pos 2	Pos 3	Pos 1	Pos 2	Pos 3
#1	140 ± 8	115 ± 8	113 ± 8	145 ± 14	121 ± 14	116 ± 14
#2	75 ± 9	77 ± 9	n.a.	75 ± 6	75 ± 6	n.a.
#3	86 ± 5	79 ± 5	78 ± 5	87 ± 4	88 ± 4	78 ± 4
#4	114 ± 6	n.a.	72 ± 6	112 ± 6	n.a.	72 ± 6
#5	126 ± 7	113 ± 7	107 ± 7	130 ± 9	114 ± 9	102 ± 9
#6	89 ± 4	93 ± 4	94 ± 4	95 ± 7	95 ± 7	93 ± 7
#7	91 ± 5	93 ± 5	67 ± 5	90 ± 4	94 ± 4	61 ± 4
#8	78 ± 3	61 ± 3	69 ± 3	79 ± 4	61 ± 4	61 ± 4
#9	90 ± 6	96 ± 6	77 ± 6	90 ± 6	96 ± 6	70 ± 6
#10	105 ± 5	84 ± 5	96 ± 5	107 ± 5	84 ± 5	88 ± 5
#11	97 ± 6	93 ± 6	67 ± 6	106 ± 5	93 ± 5	64 ± 5
#12	119 ± 7	97 ± 7	116 ± 7	120 ± 8	92 ± 8	109 ± 8
#13	102 ± 5	79 ± 5	73 ± 5	107 ± 5	81 ± 5	70 ± 5

Velocity values (cm s^{-1}) represent the root sum of squares of all velocity components and are given as mean peak velocity ± standard deviation as measured within a continuous 10 s period during free breathing. The three positions along the aortic arch are shown in Suppl. Figure S1. n.a. = not available because of incomplete coverage of the central aorta by the imaging plane.

MRI lacks access to volumetric information and therefore provides no three-dimensional visualization of complex flow phenomena. Moreover, because of anatomical variability, a cross-sectional imaging plane not always allows to cover the entire aortic arch in a similar manner, i.e. with respect to the vessel lumen. Accordingly, a corresponding flow analysis may fail to probe the correct peak velocities which for laminar flow are known to occur in the central vessel lumen. For the same reason, a cross-sectional approach does not provide flow areas and therefore precludes the evaluation of flow rates. Therefore, the proposed method for real-time multi-directional flow cannot replace established 4D flow methods, but can be seen as an additional tool with its own strengths. For example, benefits of real-time strategies are (i) the absence of phase inconsistencies when using data from multiple different heartbeats, (ii) the assessment of beat-to-beat flow variations which also allows for studies of multi-directional flow in patients with arrhythmias, (iii) the possibility to determine the influence of respiration and, in a more general context, (iv) access to the immediate physiological flow responses to breathing maneuvers or physical exercises as potential novel diagnostic stress tests. Moreover, the proposed 2d and 3d flow MRI techniques offer the potential for multi-directional flow analyses with online display and interactive slice positioning as hitherto only achieved by ultrasound technologies. As a consequence, rapid volume coverage may be accomplished by sequential multi-slice acquisitions of real-time 3d flow MRI using automatic protocols with multiple prescribed sections.

Currently, the most critical limitation of this proof-of-principle study is an offline reconstruction and the resulting lack of sufficient computational speed (about 2.5 s per frame). Although the reconstruction exhibits a significant latency, the proposed technique matches the principle requirements for real-time imaging with online display. This is because the regularized solution to the nonlinear inverse reconstruction problem of any particular frame is obtained directly after its acquisition. In fact, further progress is foreseeable by pronounced parallelization of the algorithm and its implementation on a computer with 8 graphical processing units which has already been connected to the commercial MRI system as a bypass to the vendor's reconstruction pipeline. It currently offers up to 50 fps reconstruction speed for anatomical real-time MRI and also allows for online model-based reconstruction and display of 1d flow MRI acquisitions.

6 | CONCLUSION

This study describes real-time multi-directional flow MRI by combining highly undersampled radial FLASH with model-based reconstructions based on regularized nonlinear inversion. Without the need for prospective or retrospective gating, 2d and 3d flow MRI movies of the aortic arch are achieved at a temporal resolution of 53 ms and 67 ms, respectively. These preliminary results prove the feasibility of multi-directional flow MRI in real time, while further technical progress is desirable and clinical evaluations are warranted.

ORCID

Jost M. Kollmeier ⬤ https://orcid.org/0000-0002-7568-1221
Zhengguo Tan ⬤ https://orcid.org/0000-0002-4322-5109

REFERENCES

1. Nayak KS, Nielsen JF, Bernstein MA, et al. Cardiovascular magnetic resonance phase contrast imaging. *J Cardiovasc Magn Reson*. 2015;17:71.

2. Da Silveira JS, Smyke M, Rich AV, et al. Quantification of aortic stenosis diagnostic parameters: comparison of fast 3 direction and 1 direction phase contrast CMR and transthoracic echocardiography. *J Cardiovasc Magn Reson*. 2017;19:35.

3. Steeden JA, Atkinson D, Hansen MS, Taylor AM, Muthurangu V. Rapid flow assessment of congenital heart disease with high-spatiotemporal-resolution gated spiral phase-contrast MR imaging. *Radiology*. 2011;260:79-87.

4. Hulet JP, Greiser A, Mendes JK, McGann C, Treiman G, Parker DL. Highly accelerated cardiac cine phase-contrast MRI using an undersampled radial acquisition and temporally constrained reconstruction. *J Magn Reson Imaging*. 2014;39:455-462.

5. Baltes C, Kozerke S, Hansen MS, Pruessmann KP, Tsao J, Boesiger P. Accelerating cine phase-contrast flow measurements using k-t BLAST and k-t SENSE. *Magn Reson Med*. 2005;54:1430-1438.

6. Jung B, Honal M, Ullmann P, Hennig J, Markl M. Highly k-t-space–accelerated phase-contrast MRI. *Magn Reson*. 2008;60:1169-1177.

7. Kim D, Dyvorne HA, Otazo R, Feng L, Sodickson DK, Lee VS. Accelerated phase-contrast cine MRI using k-t SPARSE-SENSE. *Magn Reson Med*. 2012;67:1054-1064.

8. Riederer SJ, Wright RC, Ehman RL, et al. Real-time interactive color flow MR imaging. *Radiology*. 1991;181:33-39.

9. Nayak KS, Pauly JM, Kerr AB, Hu BS, Nishimura DG. Real-time color flow MRI. *Magn Reson Med*. 2000;43:251-258.

10. Sun A, Zhao B, Li Y, He Q, Li R, Yuan C. Real-time phase-contrast flow cardiovascular magnetic resonance with low-rank modeling and parallel imaging. *J Cardiovasc Magn Reson*. 2017;19:19.

11. Uecker M, Hohage T, Block KT, Frahm J. Image reconstruction by regularized nonlinear inversion – joint estimation of coil sensitivities and image content. *Magn Reson Med*. 2008;60:674-682.

12. Uecker M, Zhang S, Voit D, Karaus A, Merboldt KD, Frahm J. Real-time MRI at a resolution of 20 ms. *NMR Biomed*. 2010;23:986-994.

13. Joseph AA, Merboldt KD, Voit D, et al. Real-time phase-contrast MRI of cardiovascular blood flow using undersampled radial fast low-angle shot and nonlinear inverse reconstruction. *NMR Biomed*. 2012;25:917-924.

14. Untenberger M, Tan Z, Voit D, et al. Advances in real-time phase-contrast flow MRI using asymmetric radial gradient echoes. *Magn Reson Med*. 2016;75:1901-1908.

15. Tan Z, Roeloffs V, Voit D, et al. Model-based reconstruction for real-time phase-contrast flow MRI: improved spatiotemporal accuracy. *Magn Reson Med*. 2017;77:1082-1093.

16. Bernstein MA, Shimakawa A, Pelc NJ. Minimizing TE in moment-nulled flow-encoded two- and three-dimensional gradient-echo imaging. *J Magn Reson Imaging*. 1992;2:583-588.

17. Roeloffs V, Voit D, Frahm J. Spoiling without additional gradients: radial FLASH MRI with randomized radiofrequency phases. *Magn Reson Med*. 2015;75:2094-2099.

18. Pelc NJ, Bernstein MA, Shimakawa A, Glover GH. Encoding strategies for three-dimension phase-contrast MR imaging of flow. *J Magn Reson Imaging*. 1991;1:405-413.

19. Tan Z, Hohage T, Kalentev O, et al. An eigenvalue approach for the automatic scaling of unknowns in model-based reconstructions: application to real-time phase-contrast flow MRI. *NMR Biomed*. 2017;30:e3835.

20. Rosenzweig S, Holme HCM, Uecker M. Simple auto-calibrated gradient delay estimation from few spokes using radial intersections (RING). *Magn Reson Med*. 2019;81:1898-1906.

21. Goolaub DS, Roy CW, Schrauben E, et al. Multidimensional fetal flow imaging with cardiovascular magnetic resonance: a feasibility study. *J Cardiovasc Magn Reson*. 2018;20:77.

22. Markl M, Frydrychowicz A, Kozerke S, Hope M, Wieben O. 4D flow MRI. *J Magn Reson Imaging*. 2012;36:1015-1036.

23. Stankovic Z, Allen BD, Garcia J, Jarvis KB, Markl M. 4D flow imaging with MRI. *Cardiovasc Diagn Ther*. 2014;4:173-192.

SUPPORTING INFORMATION

Additional supporting information may be found online in the Supporting Information section at the end of the article.

APPENDIX A

The three lobes of a bipolar waveform for a flow-compensated readout gradient are schematically shown in Suppl. Figure S3. The waveform for flow encoding looks similar because flow sensitivity can be included by adjusting the gradient strengths of the first and second gradient lobes. According to Bernstein et al.[16] the areas under the outer (first) and inner (second) gradient lobes for minimal timing are given by

$$A_O = -\frac{hr}{2} + \frac{1}{2}\sqrt{(hr)^2 + 2\left(hrA_R + A_R^2 + 2h(M_R + M_V)\right)}$$
$$A_I = -A_O - A_R$$

Here, h denotes the maximum gradient strength and r the minimal rise time that both constrain the gradient timing. A_R is the area under the readout gradient lobe until echo center and M_R its corresponding first gradient moment. The first gradient moment for flow encoding is given by $M_V = \frac{\pi}{\gamma\,\text{VENC}}$, whereas it is zero for flow compensation ($M_V = 0$). Thus, the minimal widths w of the outer and inner gradient lobes are defined by:

$$w_O = \frac{A_O}{h} + r$$

$$w_I = \frac{A_I}{h} + r$$

Constraining the first moments[16]

$$M_R + M_V - A_I\frac{w_I}{2} - A_O\left(w_I + \frac{w_O}{2}\right) = 0$$

the gradient strengths for the first spoke along the gradient axis are given as

$$G_O = \frac{2(M_R + M_V) + A_R w_I}{(w_O + w_I)\,(w_O - r)}$$

$$G_I = -\frac{2(M_R + M_V) + A_R(2w_I + w_O)}{(w_O + w_I)\,(w_I - r)}$$

When rotating the readout direction for radial imaging by the projection onto the x-axis, A_R and M_R are modulated by $\cos(\varphi)$, whereas M_{VENC} remains constant in order to maintain the desired flow sensitivity in x-direction.

$$G_O^x(\varphi) = \frac{2(M_R\cos(\varphi) + M_V) + A_R\cos(\varphi)w_I}{(w_O + w_I)\,(w_O - r)} = \frac{2(M_R\cos(\varphi) + [\cos[\varphi] + 1 - \cos[\varphi]]M_V) + A_R\cos(\varphi)w_I}{(w_O + w_I)\,(w_O - r)} = G_O\cos(\varphi) + \frac{2\,M_V(1 - \cos(\varphi))}{(w_O + w_I)\,(w_O - r)}\,G_I^x(\varphi)$$

$$= G_I\cos(\varphi) - \frac{2M_V(1 - \cos(\varphi))}{(w_O + w_I)\,(w_I - r)}$$